Detection of Single-base Mismatches in DNA Sequences by using Electrochemically-gated Graphene Microwave Waveguides

Patrik Gubeljak[†1], Tianhui Xu[†2,3], Lorenzo Pedrazzetti[3,4], Oliver J. Burton[3], Luca Magagnin[4], Stephan Hofmann[3], George G. Malliaras[3], and Antonio Lombardo[*1,2,5]

[1]Cambridge Graphene Centre, Department of Engineering, University of Cambridge, United Kingdom
[2]Department of Electronic and Electrical Engineering, University College London, London, United Kingdom
[3]Department of Engineering, University of Cambridge, United Kingdom
[4]Dipartimento di Chimica, Materiali e Ingegneria Chimica "Giulio Natta", Politecnico di Milano, Italy
[5]London Centre for Nanotechnology, University College London, United Kingdom

[†] These authors contributed equally to this work. *Corresponding author: a.lombardo@ucl.ac.uk

Abstract

Identification of non-amplified DNA sequences and single-base mutations is essential for molecular biology and genetic diagnostics. This paper reports a novel sensor consisting of electrochemically-gated graphene coplanar waveguides coupled with a microfluidic channel. Upon exposure to analytes, propagation of electromagnetic waves in the waveguides is modified as a result of interactions with the fringing field and modulation of graphene dynamic conductivity resulting from electrostatic gating. Probe DNA sequences are immobilised on the graphene surface, and the sensor is exposed to DNA sequences either perfectly matching the probe or containing a single-base mismatch. By monitoring the scattering parameters at frequencies between 50 MHz and 50 GHz, unambiguous and reproducible discrimination of single-base mismatch strands is achieved at concentrations as low as 1 attomole per litre (1 aM). By controlling and synchronising frequency sweeps, electrochemical gating, and liquid flow in the microfluidic channel, the sensor generates multidimensional datasets, leveraging the use of advanced data analysis techniques. By applying different machine learning methods, a classification accuracy $> 95\%$ between single-base mismatches and perfect matches is achieved, even in the presence of simulated noise and low signal-to-noise ratios. The sensor exceeds state-of-the-art sensitivity for the identification of single-base mismatches of field-effect transistors and microwave sensors.

1 Introduction

Biosensors capable of identifying non-amplified DNA sequences with high sensitivity and selectivity are essential for applications ranging from fundamental molecular biology, genetic disease diagnostic and precision medicine. Electronic detectors, such as field effect transistors (FETs), are of particular interest as they can combine label-free detection, high sensitivity, small footprint and integrability with conventional electronics for signal processing [1]. Graphene attracted significant research and commercial interest for biosensing due to its electrical and chemical properties, high surface-to-volume ratio, biocompatibility, and ease of functionalisation [2,3]. Exposure to chemical species, such as gases [4], ionic solutions [5], enzymes [6], glucose [7], large biomolecules [8], viruses [9], and bacteria [10], modifies graphene electronic properties, typically as a result of the modulation in the density and scattering rates of charge carriers. By incorporating graphene in a transistor structure, usually referred to as Graphene Field Effect Transistor (GFET) [11], the results of these interactions can be measured on a macroscopic scale, typically by monitoring changes of the charge neutrality point (CNP) in the transfer characteristics [4, 5, 12, 13]. Biomaterials are usually dispersed in a suitable medium, typically an electrolyte buffer solution. When in contact with ionic media, electrical double layers (EDLs), also known as Debye layers, form at the graphene-electrolyte interface, resulting in a large interface capacitance C_{EDL}, due to the small thickness (Debye length) of the EDL [14]. This effect is used in electrochemically-gated GFETs, where the graphene channel is exposed to the ionic solution and a voltage is applied to a counter electrode, modulating the EDL and, in turn, the charge carrier density in the graphene channel. An EDL also forms at the electrode-solution interface, leading to a capacitance

in series with C_{EDL}. However, counter-electrodes are usually designed to have areas significantly larger than the graphene channel, resulting in a very large capacitance whose effect is negligible in the series. Under such conditions, the voltage applied to the counter electrode drops almost entirely at the graphene-solution interface, i.e. across the EDL [7, 12, 13]. The total gate capacitance of electrochemically-gated GFETs, therefore, consists of graphene quantum capacitance (due to its finite density of states [15]) C_Q and EDL capacitance in series, $C_G = [C_Q^{-1} + C_{EDL}^{-1}]^{-1}$ [12]. As C_G is very large, even small changes in the solution are reflected in significant changes in the transistor transfer characteristic, resulting in very high sensitivity and low limits of detection [16]. To enhance the selectivity of GFET sensors, the graphene surface can be non-covalently functionalised with different groups, which increases the specificity while preserving the electrical conductivity [7, 12, 13].

The combination of electrochemically-gated GFETs and surface functionalisation has been applied for the identification of DNA sequences and single-base mismatches [12,13,17]. By using a binder molecule (1-pyrenebutanoic acid succinimidyl ester, PBASE), which attaches non-covalently to the graphene channel, single strands of DNA were immobilised on the GFET. When target DNA strands are introduced to the functionalised sensing surface, the hybridisation with the immobilised probe DNA modifies the potential across the EDL, resulting in shifts of the CNP [12, 13, 17]. Xu et al. [12] used this to distinguish single-base mutations quantitatively in real-time with a target DNA concentration of 5 nM based on an electrolytically gated GFET array. Campos et al. [13] improved their work and demonstrated a limit of detection (LOD) of 25 aM of the lowest target DNA concentration for which the sensor can discriminate between perfect-match sequences and nucleotides having a single base mismatch.

A major limitation of the sensitivity of field effect transistors for biosensing in physiological solutions is the ionic (Debye) shielding, which limits the detection of molecules to only those within the Debye length, i.e. usually between 0.7 and 8 nm, depending on the ionic strength of the solution. This, in turn, reduces the sensitivity, and often complex approaches are required to mitigate the screening [18]. However, the Debye shielding only affects devices operated at DC and low frequency and becomes negligible at microwave frequencies as the ionic conductivity vanishes [19]. Microwaves interact with matter causing frequency-dependent reorientation of molecular dipoles and translation of electric charges [19,20]. Different molecules and compounds are characterized by different relaxation processes (collectively captured by their dielectric permittivity) and therefore interact differently with oscillating electromagnetic fields [20]. Microwave sensors use such interaction to identify or discriminate different analytes, and have been successfully used to identify cancer cells [21], volatile compounds in breath [22], study antibiotic resistance in bacteria [23] and electroporation in human epithelial cells [24]. Different types of sensors have been reported, including reflectometers, resonators, interferometers and waveguides [20]. Waveguide sensors, such as coplanar waveguides (CPWs), are of particular interest as they combine broadband operation with simple design, ease of miniaturisation and integrability with conventional planar technology and microfluidics [19,20]. In a CPW, part of the field extends outside of the circuit due to incomplete shielding of the conductors [19, 20] and therefore interacts with analytes deposited on the waveguide surface. Yang et al. [25] developed a multilayered polymeric radio frequency (RF) for DNA sensing using a CPW sensing surface, which reached a LOD of target DNA of 10 pM through DNA hybridisation, and Kim et al. [26] proposed an RF biosensor based on an oscillator at 2.4 GHz and obtained an estimated LOD of about 1 ng/mL (114 pM).

Graphene is of particular interest for RF and microwave sensing owing to its good conductivity and field effect tunability [27–29]. Moreover, its AC conductivity is frequency-independent and equal to DC conductivity for frequencies up to $\approx$ 500 GHz [30]. This unique combination of properties has been used to demonstrate proof-of-concept electrolytically gated waveguides sensors, capable of identifying pmDNA and generating multi-dimensional datasets by independently controlling gate voltage and frequency [28]. Recently, Zhang et al. [29] reported a GFET operated around its resonant frequency (i.e., 1.83 GHz) in reflectometry mode, achieving limit-of-detection (LOD) of 1 nanomole per litre for the detection of streptavidin, an extensively used protein. Machine learning (ML) techniques play key roles in the field of biological sequencing, including DNA, RNA, and protein [31]. However, there is not much previous work using ML to analyze raw RF signals after being exposed to biological samples [32]. Principal component analysis (PCA) and quadratic discriminant analysis (QDA) have been applied to THz spectral data and achieved a classification rate of 90.3% in the prediction set of four single-base-mutation DNA oligonucleotides at a concentration of $38.85\,\mu\text{mol}\,\text{L}^{-1}$ [33].

Here we present a novel DNA sensor consisting of electrochemically-gated graphene coplanar waveguides coupled with a microfluidic channel. The sensor harnesses the combined effect of dynamic conductivity modulation in graphene resulting from (chemical) electrostatic doping and modification of wave propagation resulting from the interaction of the fringing field with the analyte. The two effect are occurring simultaneously, leading to a

unique double sensing mechanism which combines two traditionally separate sensing approaches, i.e. field effect transistors sensing and microwave dielectric spectroscopy. By immobilizing probe DNA sequences on the graphene surface, the waveguide scattering parameters are studied when the sensor is exposed to DNA sequences either perfectly matching the probe or containing a single-base mismatch, achieving unambiguous and reproducible discrimination of single-base mismatch target strands at DNA concentrations as low as 1 attomole per litre (1 aM). Multidimensional datasets are obtained by controlling and synchronising frequency sweeps, electrochemical gating, and liquid flow in the microfluidic channel. Such rich datasets are analyzed using different machine learning methods, achieving a classification accuracy $> 95\%$ between single-base mismatches and perfect matches even in the presence of simulated noise.

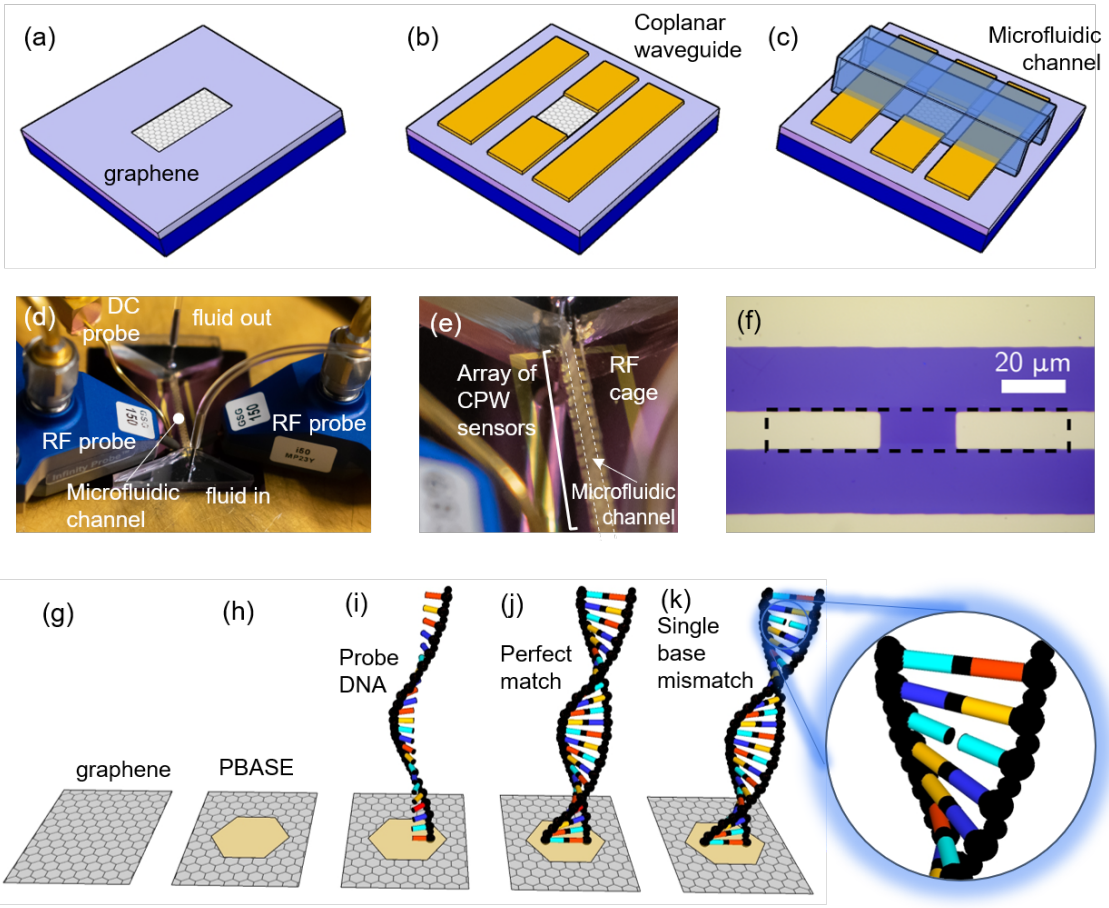

Figure 1: (a) - (c) Illustration of the steps required for a completed device. (d) Measurement setup ready for measurement. (e) Close up of the devices enclosed in the microfluidic channel and the surrounding gate electrode, doubling as an RF cage. (f) Details of the graphene section of the waveguide, with the graphene outlined in a dashed line. The overlap between the dashed line and metal is the area of the graphene-metal contacts. (g) - (k) The different chemical functionalisation and measurement stages.

2 Results and Discussion

2.1 Sensor design and sensing principle

The DNA sensor consists of a graphene channel integrated within a CPW and coupled with a microfluidic channel. The structure of the device and the main fabrication steps are schematically shown in **Figure 1 (a) - (c)**. Graphene is deposited onto high-resistivity Si substrates covered in 300nm of SiO_2 integrated in the signal track of a metallic CPW, whereas the ground conductors are entirely metallic. Arrays of sensors having different graphene lengths (ranging from 10 to 25 μm) are fabricated on the same chip and share the same microfluidic channel. A planar gold counter-electrode having dimensions significantly (> 700 times) larger than the graphene channels is fabricated on

the chip, enabling electrolytic gating similar to DC sensors [12,13]. This structure is designed to achieve a double sensing mechanism. First, electromagnetic waves propagating in the waveguide interact with the liquid in the microfluidic channel via the fringing field, i.e. the portion of the electric and magnetic field extending outside of the waveguide due to incomplete shielding of the conductors [20]. The choice of high frequencies (50 MHz - 50 GHz) ensures robustness against Debye screening, which degrades sensitivity in DC and low-frequency sensors exposed to ionic solutions such as PBS [20,29]. Second, similar to GFET sensors, the graphene's (DC and AC) conductivity is modified by the proximity with the liquid via the electrostatic effect resulting from the formation of an EDL at the graphene/solution interface [12, 13]. This further influences wave propagation, enhancing the response of the sensor. This dual sensing mechanism is fully captured by the waveguide scattering (S) parameters, which represent the ratios of the transmitted (S_{21} parameter) or reflected (S_{11} parameter) voltage wave and a known "stimulus" wave launched in the waveguide. **Figure 1 (d)** shows the chip mounted on a probe station setup, while **Figure 1 (e)** depicts a closer view of the system, showing individual devices and the microfluidic channel. **Figure 1 (f)** shows an optical micrograph of the fabricated device prior to the deposition of the microfluidic channel. The dashed area corresponds to the graphene layer, including the part underneath the contact areas. DNA sequences are immobilised onto the graphene surface by using PBASE as a linker molecule, following the protocol from Ref. [13]. The pyrene group of PBASE binds non-covalently to graphene via $\pi - \pi$ orbital stacking, whereas its succinimide group binds to the 5' end of a purposely modified single-stranded DNA, which is used as the probe, i.e. as the complementary sequence of the DNA to be detected. In order to saturate any non-reacted succinimide group, the sensor is exposed to an ethanolamine solution. The sensor containing the probe DNA is then exposed to dispersions containing either perfectly matching (pmDNA) oligonucleotides or having only a single-base mismatch (smDNA), both dispersed in 1% PBS at a concentration of 1 aM per litre. The 1% PBS concentration is chosen for consistency with previous studies on GFET-based DNA sensors [12,13], and corresponds to a Debye length of ≈ 7 nm [18], matching the length of the hybridised DNA.

Figure 1 (g) - (i) summarises the functionalisation of the sensing surface to immobilise the probe single DNA strand on the graphene surface for target DNA hybridisation, whereas (j) and (k) show hybridisation of the probe DNA with a pmDNA or smDNA, respectively. The isoelectric point of DNA is ≈ 5, while the pH of our dispersion is 7.2, resulting in the oligonucleotides being negatively charged. Upon hybridisation, i.e. when pmDNA or smDNA binds with the probe DNA by forming hydrogen bonds between complementary bases (cytosine-guanine and adenine-thymine), the additional negative change modifies the electrical double layer formed at the graphene-solution interface, leading to a lowering of the graphene's Fermi level (equivalent to p-doping) and an increase of the scattering time τ [34]. This results in a modulation of graphene dynamic conductivity, which can be described by the Kubo formula for intraband transitions [30]:

$$\sigma_{\text{intra}}\left(\omega, E_F, \tau, T\right) = \frac{\mathrm{i}e^2 k_B T}{\pi\hbar^2\left(\omega + i\tau^{-1}\right)}\left[\frac{E_F}{k_B T} + 2\ln\left(1 + \mathrm{e}^{-\frac{E_F}{k_B T}}\right)\right] \tag{1}$$

where: $\omega = 2\pi f$ is the angular frequency, E_F is the Fermi energy, τ the scattering time (assumed to be independent of energy), T is the temperature expressed in Kelvin, $e = 1.6 \cdot 10^{-19}$ C is the electron charge, $\hbar = \frac{h}{2\pi}$ is the reduced Planck's constant and $k_B = 1.38 \cdot 10^{-23}\ \frac{\text{J}}{\text{K}}$ the Boltzmann's constant.

The double helix DNA resulting from hybridisation has different electrical and mechanical properties from single-strand oligonucleotides. In particular, single-base mutations disrupt the long-range electron transfer within the DNA double-helix [35], which results in different responses to the fringing field of the propagating wave. Differences in capacitance corresponding to such mutations are also reflected in the electrostatic gating via the EDL [12, 13]. Wave propagation in the graphene waveguide captures both effects, leading to a novel sensing paradigm combining field effect sensing and dielectric spectroscopy.

2.2 DC measurements

In order to benchmark the sensors against GFET DNA detectors previously reported [12,13], the devices are first tested at DC by using the planar counter electrode as an electrolytic gate at DNA concentrations ranging from 1 aM to 100 pM. **Figure 2** shows the DC transfer characteristic of a representative sensor exposed to buffer only and after exposure to a solution of pmDNA (**Figure 2**a) and smDNA (**Figure 2**b) at concentrations varying 1 aM to pM. The devices show the typical right-shift of the charge neutrality point (CNP) with increasing concentration

for both pmDNA and smDNA [12, 13], with a possible onset of saturation at $\approx 10^{-12}$ M and limit of detection < 1 aM. The right-shift of the CNP for both pmDNA and smDNA confirms that the modulation of graphene conductivity is caused by electrostatic gating via accumulation of charges at the EDL rather than charge transfer between DNA and graphene, which would instead result in a left-shift [36]. The DC characteristic of the sensors evidences that the sensor responds to pmDNA and smDNA at all the concentration considered, outperforming state-of-the-art planar GFET sensors [13]. In the following RF and microwave investigation we focus our attention only on the smallest (and therefore most challenging) concentration, 1aM.

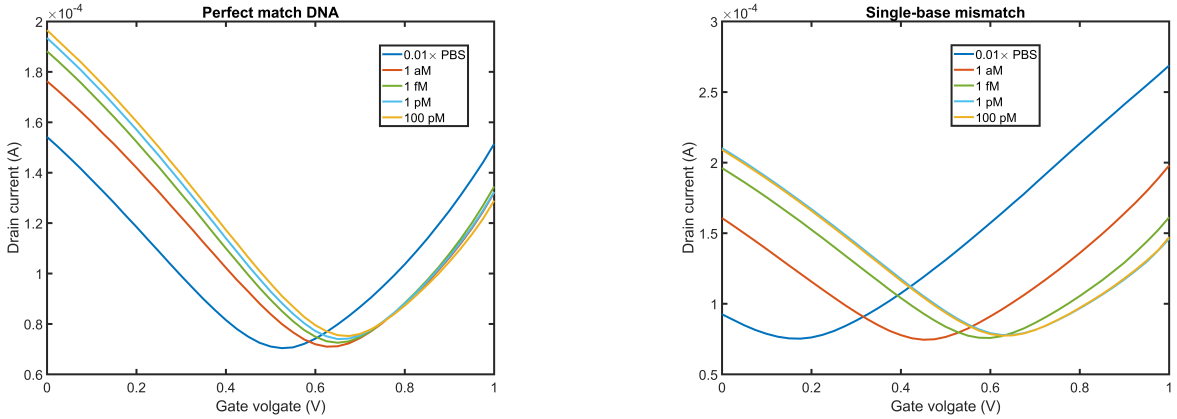

(a) (b)

Figure 2: DC transfer characteristic of the graphene sensors upon hybridization of the probe DNA with pmDNA (a) and smDNA(b) at different DNA concentrations. 0.01× PBS corresponds to the sensor exposed to buffer solution without DNA.

2.3 S-parameter measurements with no gate voltage applied

The $S-parameter$ curves of 0.01× PBS (i.e. only buffer solution with no DNA), pmDNA and smDNA at a concentration of 1 aM of a representative device are plotted in **Figure 3**. We can see distinct differences between the curves of the three solutions, especially in the case of the transmission coefficient S_{21} that contains more information on the dielectric properties of the solutions than S_{11}. To validate the reliability of the sensor for the sequence-specific detection, we investigate the performance of 13 different devices, which have the same architecture but differ in the length of the graphene channel. **Figure 4** is the bar graph of the $S-parameter$ differences at 30 GHz between buffer solution and smDNA, pmDNA, respectively. From Figure 4 we can see that different devices present consistent discriminations between the two different DNA strands. Specifically, smDNA always increases $Im(S_{21}), Amp(S_{11})$ and decreases $Re(S_{21}), Im(S_{11}), Re(S_{11}), Phase(S_{11})$, while on the contrary, pmDNA always presents opposite behaviours. $Amp(S_{21})$ increases in both smDNA and pmDNA, with the increment from pmDNA being larger than the increment from smDNA. The hybridisation of the pmDNA target with the immobilised probe introduces p-doping and result in shifting the CNP of graphene to more positive values. On the other hand, the produced duplex DNA upon hybridisation may affect the disorder of carriers and change the scattering rates of the charge carriers of graphene. In terms of smDNA, the DNA duplexes can still be formed, however they are unstable [13], leading to reduced electrostatic gating and electron transport in the oligonucleotide. As a result, pmDNA and smDNA modify the carrier density and the dielectric properties at the interface differently, leading to the differences in the changes of the electrical conductance of graphene and the total capacitance of the channel. These differences impact the transmission and reflection of microwave, which are fully captured by $S-parameters$.

Therefore, the observed differences in the $S-parameters$ indicate that the sensor is highly selective of the two kinds of DNA strands, and this result possesses high reliability among multiple devices. In addition, a linear fitting between the graphene channel lengths and the logarithmic (dB) S_{21} at 30 GHz is shown in **Figure 5**. The logarithmic S_{21} for each graphene length is calculated as the average of the dB values of 3 different devices with the same graphene lengths. The good linearity between the logarithmic S_{21} and the graphene channel lengths demonstrates the uniformity of the graphene and of the contact resistance. In addition, p-values [37], which

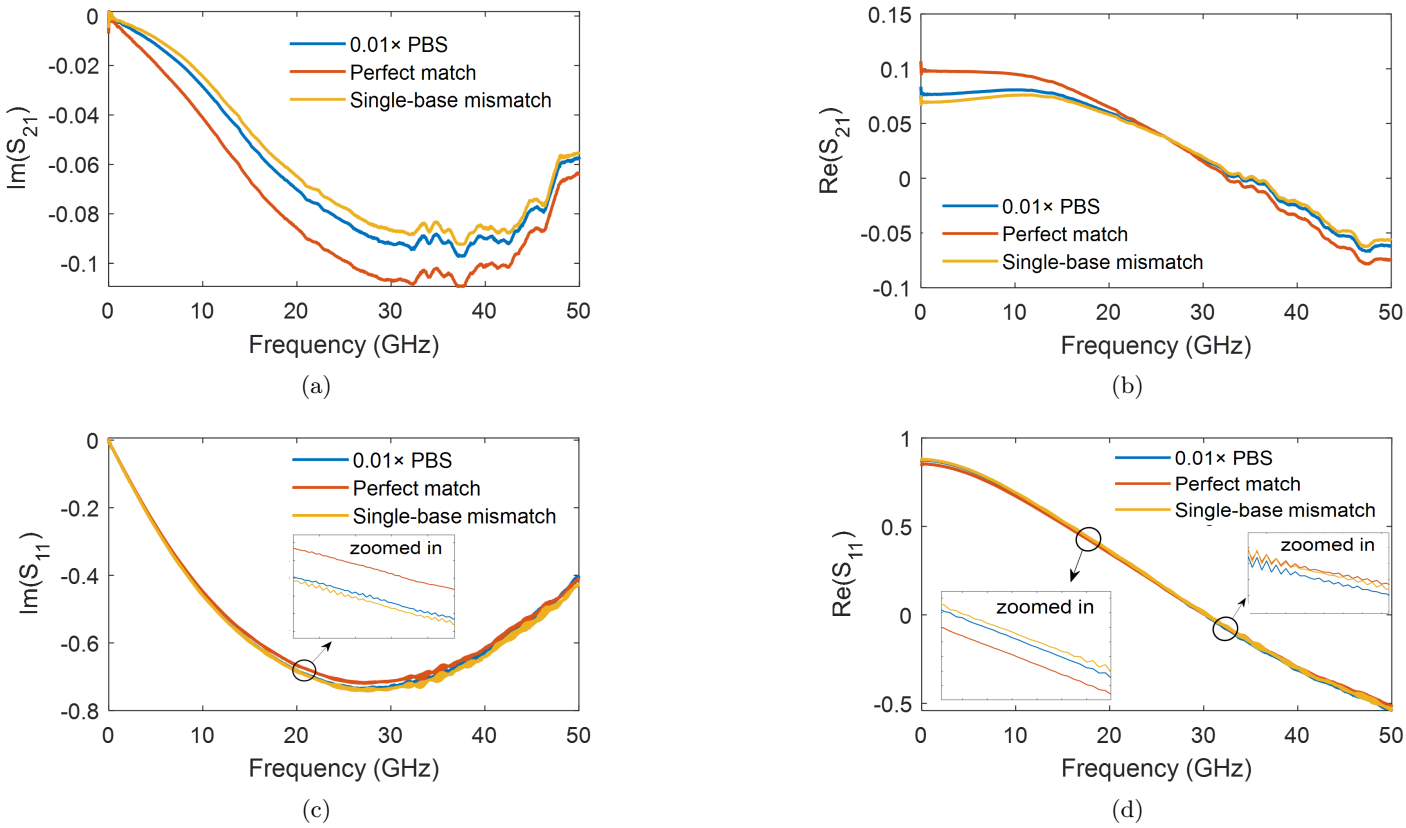

Figure 3: A representative set of $S-parameter$ curves for a specific device for 0.01× PBS, pmDNA and smDNA. (a) Imaginary part of S_{21} (b) Real part of S_{21} (c) Imaginary part of S_{11} (d) Real part of S_{11}. DNA concentration is 1 aM. The different colours represent different solution classes.

can present the probability that the differences between pmDNA data and smDNA data occur by chance, are calculated to quantitatively evaluate the distinctions in the signal between the two classes. The mean p-value of 13 different devices for the S_{21} (dB) at 9 different DNA concentrations (1 aM, 10 aM, 100 aM, 1 fM, ..., 100 pM) at one frequency between the two DNA classes is $0.042 < 0.05$, which demonstrates a significant difference between the data vectors of the two classes at a confidence level of 95%. Therefore, this quantitative result also showcases the sensor's robust selectivity between the two DNA strand classes. Especially, one of the devices with a graphene length of 25 µm has a superior selectivity between the two classes at 35.45 GHz, with a p-value of $0.000216 < 0.0001$ (a confidence level of 99.99%).

2.4 Multidimensional approach

To analyse the effects of different gate voltage biases, we observe the $S-parameters$ measured with gate voltage V_{GS} sweep. **Figure 6b** and **Figure 6a** exhibit the S_{21} curves against different gate voltage V_{GS} at 6 discrete frequencies for smDNA and pmDNA, respectively. It can be observed that, as expected, the S_{21} (dB) presents a V-shaped trend simular to the DC transfer curves of the device, and the V_{GS} at which the S_{21} (dB) reach minima for smDNA and pmDNA is different due to the differences in ΔV_{CNP} upon DNA binding. Also, the S_{21} curves against different frequencies at 5 different gate voltages in **Figure 6d** and **Figure 6c** demonstrate similar trends but distinctions in fluctuations and different amplitudes at each gate voltage for smDNA and pmDNA. Our design allows independent sweeping of electrolyte gating and wave frequency, which results in information-rich $V_{GS}-Frequency$ surfaces of $S-parameters$. **Figure 6f** and **Figure 6e** present the $V_{GS}-Frequency$ 3D plots of the S_{21} for pmDNA and smDNA at a concentration of 1 aM of one device. Gate voltage sweep and frequency sweep introduce richer information that combines the above variations of the measurements at only one frequency or with no gate voltage biases. As a result, differing from single GFET sensing and single microwave sensing, the response is a combined effect of the changes in graphene conductivity, channel capacitance, and the dielectric properties of the solutions. The resulting variations in the maxima, minima and gradients of the surfaces offer insights into the

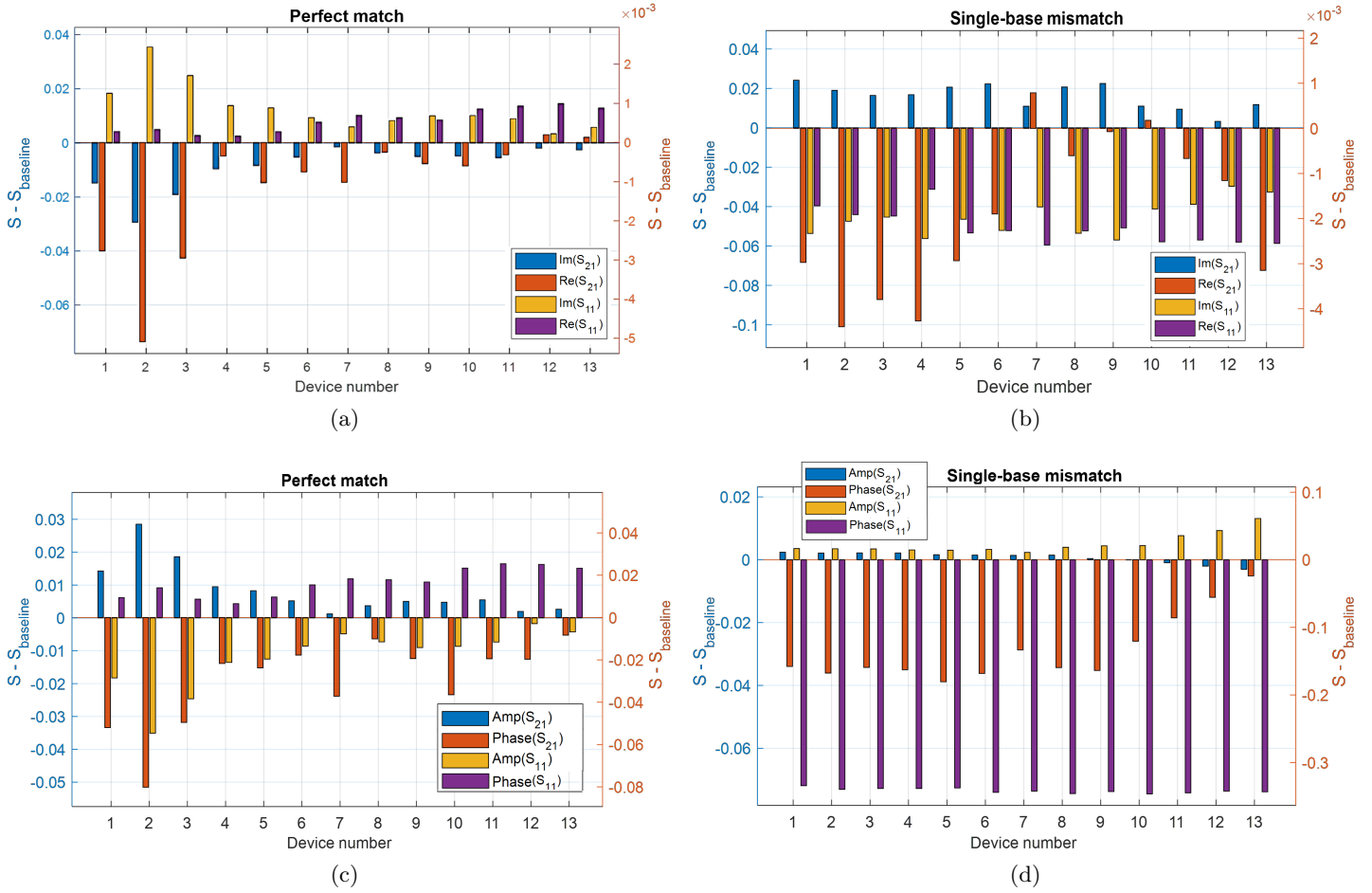

Figure 4: Bar graphs of the differences in the real, imaginary, amplitude, phase of S_{21} and S_{11} between the PBS baseline and pmDNA, smDNA, respectively, for each device (numbered from 1 to 13) in the array. The frequency is 30 GHz, at which the $Im(S_{21})$ in Figure 3 presents a clear difference between the three different solutions. DNA concentration is 1 aM. The different colours represent different $S-parameter$ parts. For better visualisation, the y-axis on the left corresponds to the blue, yellow, and purple components, while the y-axis on the right is for the orange component.

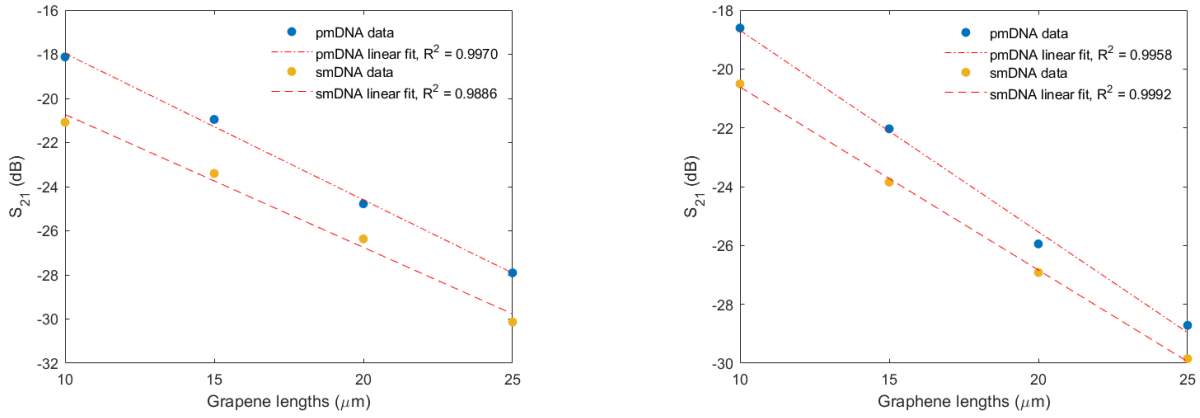

Figure 5: Scatter plots and linear-fit curves of S_{21} (dB) against graphene channel lengths for pmDNA and smDNA. (a) 50 MHz (b) 30 GHz. DNA concentration is 1 aM. The good linearity corresponds well with theoretical expectations, which validates the reliability of the sensor measurements.

electrochemical behaviour of different DNA solutions. Therefore, these observations indicate a good sensitivity of the sensor in detecting the DNA strands at a concentration of 1 aM, and the clear distinctions between the two 3D plots visually illustrate the good selectivity of the sensor between the pmDNA and smDNA under test. Furthermore, the information dimensionality can be even higher due to the complex values of $S-parameters$, specifically, $[Re(S_{xy}) \quad Im(S_{xy})]$ or $[|S_{xy}| \quad \angle S_{xy}]$. As a result, the high-dimensional information and the non-linear behaviors of the sensor encourage the usage of advanced data analysis techniques to obtain quantifiable results and practical solutions for practical biosensing purposes.

2.5 Classification between single-base mismatch DNA and perfect-match DNA with ML

When considering the whole data obtained with different gate voltage biases, the $V_{GS}-Frequency$ 3D plots of the S_{21} (dB) for the two different DNA classes in Figure 6 exhibit rich but complex variations, which are non-trivial to analyse with conventional analogue, statistical or mathematical methods. In this case, we utilise ML as a data analysis method, and we consider the binary classification task between the smDNA and pmDNA. Multiclass classification is also considered, separating the nine pmDNA solutions that have nine different concentrations. The dataset for ML is constructed with the four components of S_{11} and S_{21}; $[Re(S_{11}) \quad Im(S_{11})]$ and $[Re(S_{21}) \quad Im(S_{21})]$ over the whole frequency range and the whole gate voltage range at a specific DNA concentration. Specifically, each set of $S-parameter$ parts at each gate voltage for each device is a sample. In total, we use 41×7 samples at 41 different electrolytic gate biases from 1 V to 0 V and 7 different devices for each class, and each sample has 1001×4 features obtained from the 4 $S-parameter$ parts at 1001 different frequency points from 50 MHz to 50 GHz. To reduce feature dimensions, PCA is utilised, and nine principal components are constructed with a variance of 99%. The final dataset has a dimension of 574×9. This dataset is split into a training set (80%) and a testing set (20%), and a validation set is created during training based on different criteria for different algorithms. Popular classification models are implemented on the dataset using MATLAB Classification Learner. The Linear Discriminant Analysis (LDA) has a linear coefficient threshold of 0 and no regularisation. The Support Vector Machine (SVM) has a linear kernel with a box constraint value of 1. The Decision Tree has a maximal number of 100 decision splits. The number of neighbours of the k-nearest neighbours (KNN) is set to 1, with euclidean distance and no distance weight. All the models finish training within 6 s of running on a single core of an Intel i7-10750H CPU. **Table 1** presents the testing result of different ML models. The accuracy is the average of nine accuracy for nine different DNA concentrations. In addition to the original signal, Gaussian noise with a signal-to-noise ratio (SNR) of 10 dB is added to the signal to test the robustness of the models. We can see that all the models present high testing accuracy $> 97\%$ for the original signal. After adding noise to the signal, all the accuracy decreased but is still reasonably good, except for KNN and Gaussian Naive Bayes, which may be attributed to the high variance of model predictions. The testing result of the classification of pmDNA with nine different solution concentrations is similar to the binary classification task for the original signal and for the added-noise signal with a smaller noise level of 30 dB SNR. The Artificial Neural Network (ANN) has an input layer of 4004 and two hidden layers with 20 neurons, each followed by a ReLU activation function, and a Softmax layer is added at last for cross-entropy loss calculation. The network is trained with SGDM Optimiser, with a learning rate of 0.005 and a mini-batch size of 64. The model is implemented using MATLAB Deep Network Designer. **Figure 7** demonstrates the accuracy and loss curves of training and validation of the ANN model. After around 5 seconds of training, the training accuracy converges to 100% at around 50^{th} iteration; a similar trend is presented in the validation curve, with a final accuracy of 100% and loss equal to 0.023, which attests to the model's low variance.

The concept of uncertainty has been understudied in the ML context [38], but is highly relevant for developing measurement methods. Generally, the variance of outputs is used as a measure of uncertainty [39]. Due to the Softmax probability output, data uncertainty can be quantified for the classification tasks, and the correlation between cross-entropy loss and the entropy of Softmax output can be calculated to evaluate the uncertainty estimates of the results. A well-calibrated metric should predict credibility (uncertainty) approximate to accuracy (error) [40]. The mean uncertainty estimated by the entropy of Softmax output of the binary classification results at nine concentrations is 0.118 bit, with a high mean correlation value of 0.978. **Figure 8a** indicates that the two quantities correlate well with each other. Hence, the uncertainty estimate can be useful for monitoring the performance of the model [41]. However, we see variations in the uncertainty estimation at different DNA concentrations, for instance, a higher correlation between uncertainty and loss for the predictions at 1 aM than 10

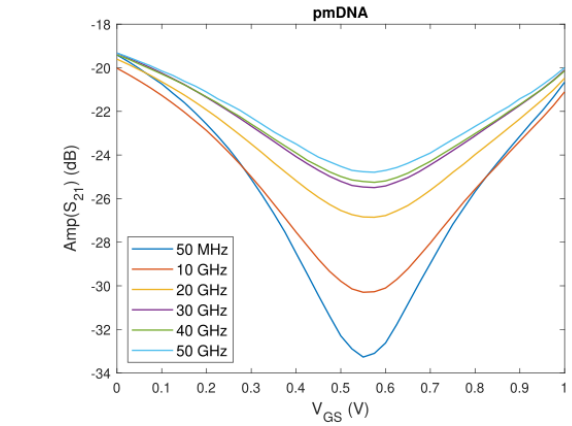

(a)

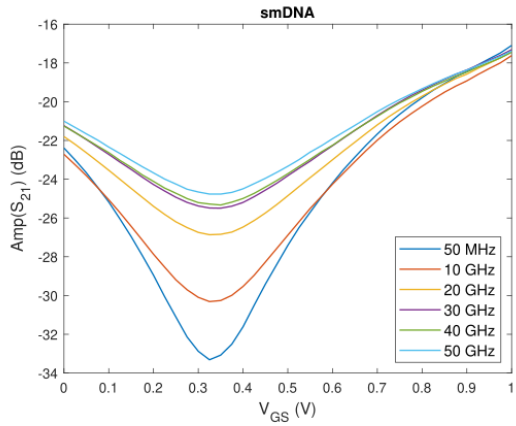

(b)

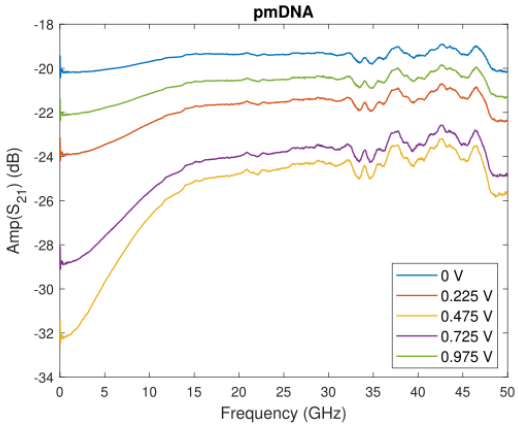

(c)

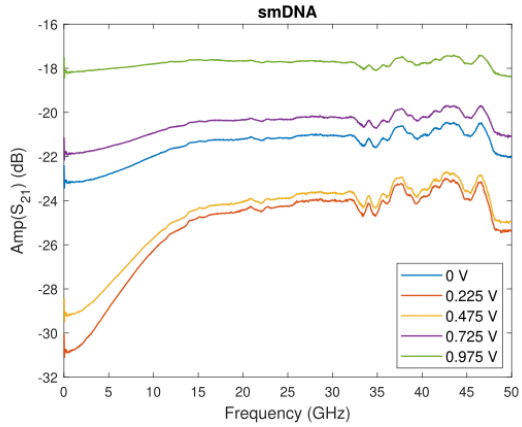

(d)

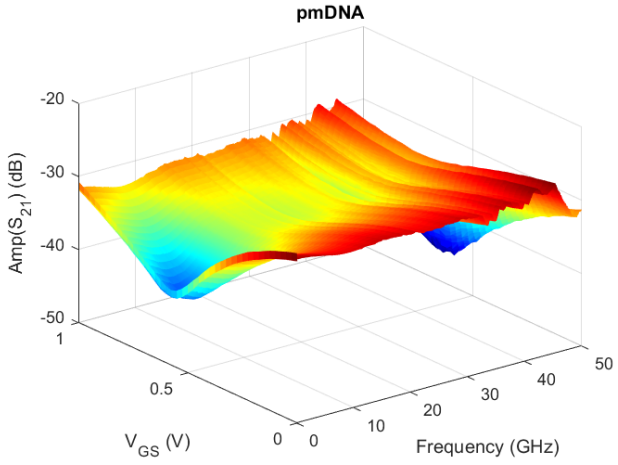

(e)

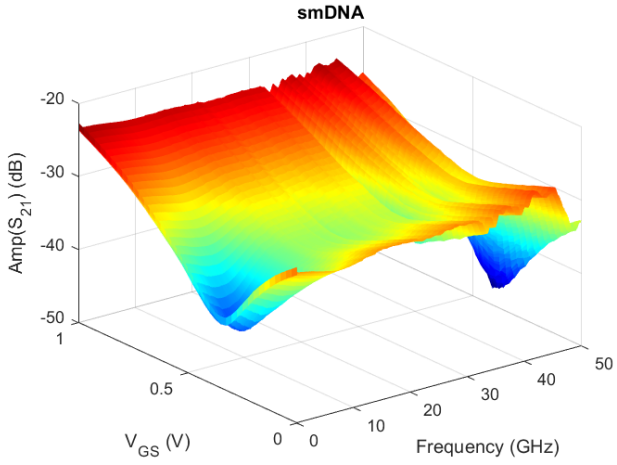

(f)

Figure 6: $S_{21}\,(dB) - gate\,voltage\,V_{GS}$ curves at different frequencies for (a) smDNA and (b) pmDNA. $S_{21}\,(dB) - Frequency$ curves at different gate voltages for (c) smDNA and (d) pmDNA. $S_{21}\,(dB) - V_{GS} - Frequency$ 3D plots for (e) smDNA and (f) pmDNA. The axes in (e) and (f) have the same limits. Variations can be observed as different features at different frequencies and gate voltages on each surface, as well as the differences between the two complete surfaces.

pM. Therefore, it is worth pursuing uncertainty quantification approaches with a better generalisation that can evaluate both data and model uncertainty [42]. In addition to adding Gaussian noise to the signal, a method based on uncertainty evaluation is also conducted to examine the performance of the ANN model. A robust model should

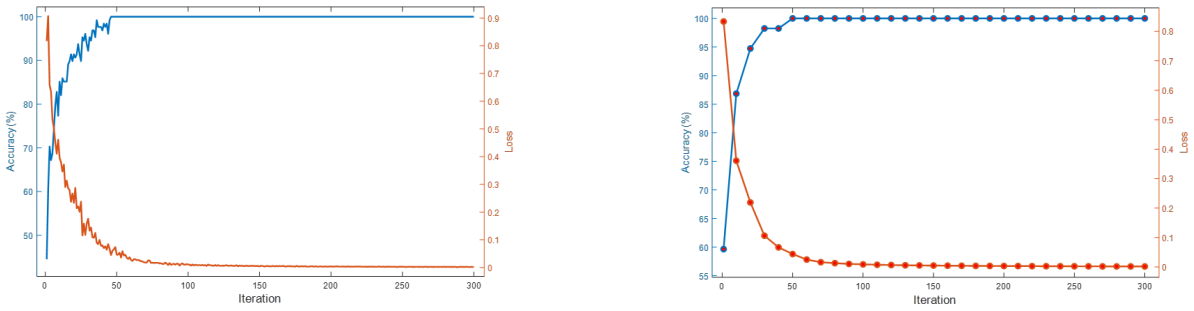

(a) Training curves

(b) Validation curves

Figure 7: Accuracy and Loss curves of Training and Validation of ANN. Both validation and training accuracy increase with iterations and converge to 100%.

Table 1: ML model classification performance

Algorithms	Accuracy (%)	Accuracy with noise (%)
Logistic Regression	99.81	94.74
LDA	98.73	95.05
ANN	99.31	91.23
SVM	99.90	89.17
Tree	99.32	84.55
Gaussian Naive Bayes	98.35	73.25
KNN	97.90	32.36

output high predictive uncertainty if the input is unknown [43]. The histogram of the Softmax entropy uncertainty score on test examples from known classes (pmDNA and smDNA) and the unknown class (post-ethanolamine) is shown in **Figure 8b**. We can observe a clear increase in the output entropy when the model handles the unknown data, which validates the credible predictions for the known two classes of DNA. The ability of ML models to distinguish out-of-distribution examples is critical for applications in practical systems. By using ML we achieve high accuracy and reliability in the detection of single-base mismatch based on the RF signal measured with the graphene microwave sensor, and the models are applicable to the data measured with different gate voltage biases from 0 V to 1 V. We note that experimental data does not require precise and complicated calibrations and de-embedding before being fed to ML models for training and predictions, which reduce experimental work and artifacts and thus increase efficiency and accuracy. Moreover, the short training time of ML models and the advantage in predicting new data using the trained models instantly make ML well-suited for real-time applications.

3 Conclusions

We presented a novel DNA sensor consisting of electrochemically-gated graphene coplanar waveguides coupled with microfluidic channels. By immobilising probe DNA sequences on the graphene surface and exposing the sensor to either pmDNA or smDNA, we achieve consistent and reproducible identification of single-base mismatch at DNA concentrations as low as 1 aM. The possibility of independently controlling gate voltage and frequency sweeps lead to multidimensional datasets, which are analysed using ML learning methods, achieving a classification accuracy $> 95\%$ between single-base mismatch and perfect match, even in the presence of simulated noises. The device concept presented here goes beyond DNA sensing, paving the way for a generally-applicable approach to biosensing, where chemical field-effect sensing and microwave impedance spectroscopy are combined in a single platform.

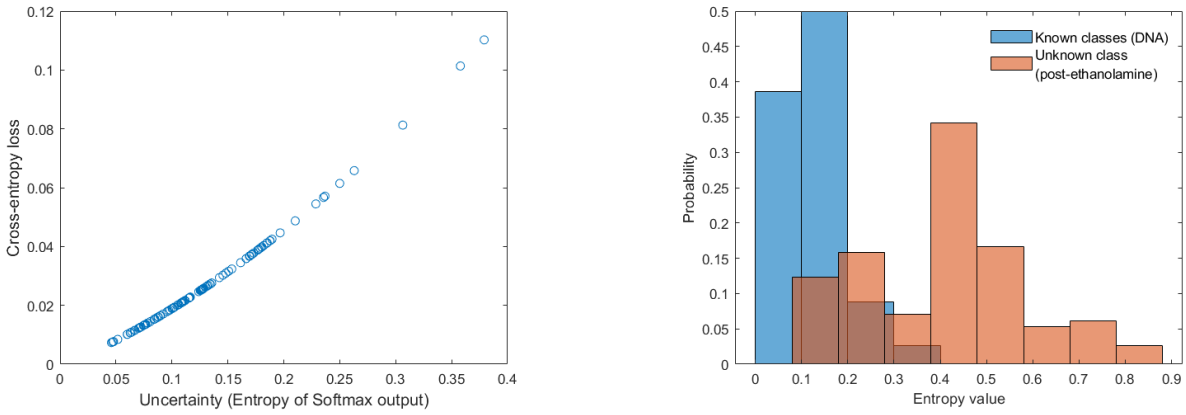

(a) (b)

Figure 8: Uncertainty evaluation of ANN predictions. (a) Correlation scatter plot between the entropy of Softmax output (uncertainty) and the cross-entropy loss. Each dot represents a sample. (b) Histogram of the predictive entropy on testing datasets from known DNA data and unknown post-ethanolamine data.

4 Methods

4.1 Graphene synthesis and transfer

Graphene layers are grown via Chemical Vapour Deposition (CVD) on Cu foil, following the protocol developed by Burton et al [44]. The foil is heated to a high temperature, and hydrogen and methane gases are introduced. The copper foil acts as both the catalyst and the substrate for the deposition. Graphene is transferred onto high-resistivity Si substrates ($\rho > 10,000 \Omega cm$) covered in 300 nm-thick thermally-grown oxide by using a sacrificial layer of polymethyl methacrylate (PMMA) 495K (8% in anisole, MicroChem), deposited onto the graphene-coated Cu foil via spin-coating. After exposing the bottom side of the Cu foil to oxygen plasma (10 W, 60 s), the PMMA/graphene/Cu stack is then floated on a 0.5 m% solution of $(NH_4)_2S_2O_8$ overnight. This etches away the metal layer, leaving the graphene-PMMA stack floating on the surface. This stack is then picked up and re-floated on top of DI water to remove metal and etchant residue. To ensure good adhesion between the graphene and the substrate as well as reduce the interaction with the Si-O-H groups on the surface, any trapped water and the graphene, the wafer was primed using Hexamethyldisilazane (HMDS). The wafer is then used to lift the graphene-PMMA stack of the DI water surface and left to dry naturally overnight. The sacrificial PMMA is removed by two consecutive acetone baths and an isopropanol bath. After the PMMA removal, the graphene on the Si substrate is heated to 150 °C for 5 minutes to drive out any residual moisture trapped between the substrate and graphene.

4.2 Design and fabrication

The largest part of the CPW, which feeds the signal to the graphene channel, is designed to match Ground-Signal-Ground (GSG) probes with 150 μm pitch per manufacturer specification [45]. For better adhesion of the microfluidic polydimethylsiloxane (PDMS) channel, the metal part of the waveguide is extended to maximise the contact area between PDMA and the substrate. The GFET is incorporated by tapering the central trace of the waveguide and adjusting the separation between the G and S conductors so that the characteristic impedance is close to 50 Ω, matching the rest of the measurement system. Most graphene FET devices, including state-of-the-art sensors, use a graphene-on-top design. The advantage of our approach is the ability to pre-treat the graphene-metal contact area prior to deposition to improve the contact resistance, especially important for RF devices [46, 47]. The increased length of the contact area beyond that of typical DC devices also increases the capacitive coupling between the metal leads and the graphene channel, resulting in lower insertion loss in comparison with previous efforts [28]. The dried graphene is patterned using direct-write laser lithography, and the excess material is etched by reactive ion etching using 3 W oxygen plasma for 30 seconds. The metal layer is patterned with a long overlap between the exposed graphene. Directly prior to metal deposition, we expose the contact area using a 0.5 W argon plasma for 20 seconds to improve our contact resistance. We use 5 nm Cr as the adhesion layer and deposit a

further 100 nm of gold using an e-beam evaporator followed by liftoff in acetone. The microfluidic channel was made using PDMS from an SU-8 epoxy mould and mounted to the patterned CPW structures. To connect the device assembly to the microfluidic controller, feedlines were introduced and the entry points were sealed using liquid PDMS. To bond the PDMS to the wafer better and cure the fluid inlet seals, we cured the entire assembly at 80 °C overnight.

4.3 Functionalisation

We use the microfluidic assembly to passivate and functionalise the metal and graphene areas of the CPWs, respectively. First, the Au is passivated using a solution of 1-dodecanethiol, as oligonucleotides have an affinity for Au. Then, the linker molecule, PBASE, is introduced and left for 2 hours to interact with the graphene, after which the channel is rinsed using methanol. This allows us to immobilise a probe single DNA strand consisting of 20 bases (P20) on the graphene surface using the added amine (NH_2-) group by exposing the graphene channel to a slow flow (0.5 μL/min) of a 10 pM dispersion of P20 in a 1% phosphate buffer solution (0.01× PBS) for 12 hours. To prevent any unreacted PBASE sites from reacting with our target oligonucleotides (pmDNA and smDNA), we passivate them using a 0.1 M ethanolamine solution in 0.01× PBS for 30 min. The post-ethanolamine measurement thus forms our baseline for comparing all other data.

4.4 Measurements

For DC and RF characterisation, we mount the sample on a Cascade Microtech Summit 12000B semi-automatic probe station. An Agilent PNA-X 5245 vector network analyser (VNA) is connected to a pair of Cascade Microtech i50 GSG 150 Infinity probes, which we calibrate using a manufacturer-provided impedance standard substrate (ISS) via the mTRL method. For DC measurements and electrolytic gating, we use an Agilent B1500A Parameter Analyser, connected to the RF probes using a biasing network and to the gate electrode using a Cascade Microtech DCP100 probe, as shown in Figure 1 (d) & (e). We used an RF power of -12 dBm and an IF of 1 kHz, with 1001 points collected between 50 MHz and 50 GHz. The fluid flow is controlled by an ElveFlow OB1+ Mk3 microfluidic controller. Each analyte, i.e. dispersions of different concentrations of pmDNA or single smDNA, is introduced by setting the flow to 1 μL/min and reacting for 60 minutes, after which the channel is rinsed with 0.01× PBS for 10 minutes. All measurements are performed with 0.01× PBS flowing into the channel at 1 μL/min. We started by measuring all concentrations of the perfect match DNA dispersions from lowest to highest, followed by a 0.1 M NaOH solution and buffer rinse, to recover the pristine probe DNA sites, as per [12]. The matching concentrations of smDNA were then introduced and measured in the same manner. As GFETs often exhibit hysteresis, we swept the gate voltage from 0 V to 1 V 10 times to stabilise the transfer curves, after which the S-parameters are measured. To accurately and repeatably measure the array of devices, we developed automated control scripts to perform DC measurements, synchronise S-parameter measurements with the applied electrolytic gate bias and characterise the entire wafer.

Acknowledgements
This work is supported by EPSRC grant EP/L016087/1.

References

[1] D. Sadighbayan, M. Hasanzadeh, and E. Ghafar-Zadeh, "Biosensing based on field-effect transistors (fet): Recent progress and challenges," *TrAC Trends in Analytical Chemistry*, vol. 133, p. 116067, 2020.

[2] D. Bitounis, H. Ali-Boucetta, B. H. Hong, D.-H. Min, and K. Kostarelos, "Prospects and challenges of graphene in biomedical applications," *Advanced Materials*, vol. 25, no. 16, pp. 2258–2268, 2013.

[3] I. Prattis, E. Hui, P. Gubeljak, G. S. Kaminski Schierle, A. Lombardo, and L. G. Occhipinti, "Graphene for biosensing applications in point-of-care testing," *Trends in Biotechnology*, vol. 39, no. 10, pp. 1065–1077, 2021.

[4] F. Schedin, A. K. Geim, S. V. Morozov, E. W. Hill, P. Blake, M. I. Katsnelson, and K. S. Novoselov, "Detection of individual gas molecules adsorbed on graphene," *Nature Materials*, vol. 6, pp. 652–655, July 2007.

[5] H. Li, Y. Zhu, M. S. Islam, M. A. Rahman, K. B. Walsh, and G. Koley, "Graphene field effect transistors for highly sensitive and selective detection of k+ ions," *Sensors and Actuators B: Chemical*, vol. 253, pp. 759–765, 2017.

[6] L. Fritea, M. Tertis, R. Sandulescu, and C. Cristea, "Chapter eleven - enzyme–graphene platforms for electrochemical biosensor design with biomedical applications," in *Enzyme Nanoarchitectures: Enzymes Armored with Graphene* (C. V. Kumar, ed.), vol. 609 of *Methods in Enzymology*, pp. 293 – 333, Academic Press, 2018.

[7] M. Zhang, C. Liao, C. H. Mak, P. You, C. L. Mak, and F. Yan, "Highly sensitive glucose sensors based on enzyme-modified whole-graphene solution-gated transistors," *Sci Rep*, vol. 5, p. 8311, 2015. Zhang, Meng Liao, Caizhi Mak, Chun Hin You, Peng Mak, Chee Leung Yan, Feng eng Research Support, Non-U.S. Gov't England 2015/02/07 06:00 Sci Rep. 2015 Feb 6;5:8311. doi: 10.1038/srep08311.

[8] A. Bharti, S. Rana, D. Dahiya, N. Agnihotri, and N. Prabhakar, "An electrochemical aptasensor for analysis of MUC1 using gold platinum bimetallic nanoparticles deposited carboxylated graphene oxide," *Analytica Chimica Acta*, vol. 1097, pp. 186–195, Feb 2020.

[9] G. Seo, G. Lee, M. J. Kim, S.-H. H. Baek, M. Choi, K. B. Ku, C.-S. S. Lee, S. Jun, D. Park, H. G. Kim, S. J. S. I. S.-J. Kim, J.-O. O. Lee, B. T. Kim, E. C. Park, and S. J. S. I. S.-J. Kim, "Rapid Detection of COVID-19 Causative Virus (SARS-CoV-2) in Human Nasopharyngeal Swab Specimens Using Field-Effect Transistor-Based Biosensor," *ACS nano*, vol. 14, pp. 5135–5142, Apr 2020.

[10] N. Mohanty and V. Berry, "Graphene-based single-bacterium resolution biodevice and dna transistor: Interfacing graphene derivatives with nanoscale and microscale biocomponents," *Nano Letters*, vol. 8, no. 12, pp. 4469–4476, 2008. PMID: 18983201.

[11] K. S. Novoselov, A. K. Geim, S. V. Morozov, D. Jiang, Y. Zhang, S. V. D. vand I. V. Grigorieva, and A. A. Firsov, "Electric field effect in atomically thin carbon films," *Science*, vol. 306, pp. 666–669, 10 2004.

[12] S. Xu, J. Zhan, B. Man, S. Jiang, W. Yue, S. Gao, C. Guo, H. Liu, Z. Li, J. Wang, and Y. Zhou, "Real-time reliable determination of binding kinetics of DNA hybridization using a multi-channel graphene biosensor," *Nature Communications*, vol. 8, Mar. 2017.

[13] R. Campos, J. Borme, J. R. Guerreiro, G. Machado, M. F. Cerqueira, D. Y. Petrovykh, and P. Alpuim, "Attomolar label-free detection of DNA hybridization with electrolyte-gated graphene field-effect transistors," *ACS Sensors*, vol. 4, pp. 286–293, Jan. 2019.

[14] A. Das, S. Pisana, B. Chakraborty, S. Piscanec, S. K. Saha, U. V. Waghmare, K. S. Novoselov, H. R. Krishnamurthy, A. K. Geim, A. C. Ferrari, and A. K. Sood, "Monitoring dopants by raman scattering in an electrochemically top-gated graphene transistor," *Nature Nanotechnology*, vol. 3, pp. 210–215, Mar. 2008.

[15] J. Fernández-Rossier, J. J. Palacios, and L. Brey, "Electronic structure of gated graphene and graphene ribbons," *Phys. Rev. B*, vol. 75, p. 205441, May 2007.

[16] M. T. Hwang, M. Heiranian, Y. Kim, S. You, J. Leem, A. Taqieddin, V. Faramarzi, Y. Jing, I. Park, A. M. van der Zande, S. Nam, N. R. Aluru, and R. Bashir, "Ultrasensitive detection of nucleic acids using deformed graphene channel field effect biosensors," *Nature Communications*, vol. 11, Mar. 2020.

[17] M. T. Hwang, P. B. Landon, J. Lee, D. Choi, A. H. Mo, G. Glinsky, and R. Lal, "Highly specific SNP detection using 2d graphene electronics and DNA strand displacement," *Proceedings of the National Academy of Sciences*, vol. 113, pp. 7088–7093, June 2016.

[18] N. Nakatsuka, K.-A. Yang, J. M. Abendroth, K. M. Cheung, X. Xu, H. Yang, C. Zhao, B. Zhu, Y. S. Rim, Y. Yang, P. S. Weiss, M. N. Stojanović, and A. M. Andrews, "Aptamer–field-effect transistors overcome debye length limitations for small-molecule sensing," *Science*, vol. 362, no. 6412, pp. 319–324, 2018.

[19] F. Artis, T. Chen, T. Chretiennot, J.-J. Fournie, M. Poupot, D. Dubuc, and K. Grenier, "Microwaving biological cells: Intracellular analysis with microwave dielectric spectroscopy," *IEEE Microwave Magazine*, vol. 16, pp. 87–96, 5 2015.

[20] G. Guarin, M. Hofmann, J. Nehring, R. Weigel, G. Fischer, and D. Kissinger, "Miniature microwave biosensors: Noninvasive applications," *IEEE Microwave Magazine*, vol. 16, no. 4, pp. 71–86, 2015.

[21] K. Grenier, D. Dubuc, T. Chen, F. Artis, T. Chretiennot, M. Poupot, and J.-J. Fournie, "Recent advances in microwave-based dielectric spectroscopy at the cellular level for cancer investigations," *IEEE Transactions on Microwave Theory and Techniques*, vol. 61, no. 5, pp. 2023–2030, 2013.

[22] K. Schmalz, N. Rothbart, P. F. X. Neumaier, J. Borngraber, H.-W. Hubers, and D. Kissinger, "Gas spectroscopy system for breath analysis at mm-wave/thz using sige bicmos circuits," *IEEE Transactions on Microwave Theory and Techniques*, vol. 65, no. 5, pp. 1807–1818, 2017.

[23] M. C. Jain, A. V. Nadaraja, R. Narang, and M. H. Zarifi, "Rapid and real-time monitoring of bacterial growth against antibiotics in solid growth medium using a contactless planar microwave resonator sensor," *Scientific Reports*, vol. 11, no. 1, 2021.

[24] A. Tamra, D. Dubuc, M.-P. Rols, and K. Grenier, "Evaluation of a microwave biosensor for on-chip electroporation and efficient molecular delivery into mammalian cells," *IEEE Journal of Electromagnetics, RF and Microwaves in Medicine and Biology*, vol. 3, no. 3, pp. 224–231, 2019.

[25] C.-H. Yang, L.-S. Kuo, P.-H. Chen, C.-R. Yang, and Z.-M. Tsai, "Development of a multilayered polymeric dna biosensor using radio frequency technology with gold and magnetic nanoparticles," *Biosensors and Bioelectronics*, vol. 31, no. 1, pp. 349–356, 2012.

[26] S.-G. Kim, H.-J. Lee, J.-H. Lee, H.-I. Jung, and J.-G. Yook, "A highly sensitive and label free biosensing platform for wireless sensor node system," *Biosensors and Bioelectronics*, vol. 50, pp. 362–367, 2013.

[27] F. Schwierz, "Graphene transistors," *Nature nanotechnology*, vol. 5, no. 7, pp. 487–496, 2010.

[28] P. Gubeljak, L. Pedrazzetti, O. J. Burton, L. Magagnin, S. Hofmann, G. G. Malliaras, and A. Lombardo, "Multi-dimensional microwave sensing using graphene waveguides," in *2022 IEEE International Symposium on Medical Measurements and Applications (MeMeA)*, pp. 1–6, 2022.

[29] X. Zhang, T. Liu, A. Boyle, A. Bahreman, L. Bao, Q. Jing, H. Xue, R. Kieltyka, A. Kros, G. F. Schneider, *et al.*, "Dielectric-modulated biosensing with ultrahigh-frequency-operated graphene field-effect transistors," *Advanced Materials*, vol. 34, no. 7, p. 2106666, 2022.

[30] S. A. Awan, A. Lombardo, A. Colli, G. Privitera, T. S. Kulmala, J. M. Kivioja, M. Koshino, and A. C. Ferrari, "Transport conductivity of graphene at RF and microwave frequencies," *2D Materials*, vol. 3, p. 015010, Feb. 2016.

[31] B. Liu, "BioSeq-Analysis: a platform for DNA, RNA and protein sequence analysis based on machine learning approaches," *Briefings in Bioinformatics*, vol. 20, pp. 1280–1294, 12 2017.

[32] J. C. Soares, A. C. Soares, V. C. Rodrigues, P. R. A. Oiticica, P. A. Raymundo-Pereira, J. L. Bott-Neto, L. A. Buscaglia, L. D. C. de Castro, L. C. Ribas, L. Scabini, L. C. Brazaca, D. S. Correa, L. H. C. Mattoso, M. C. F. de Oliveira, A. C. P. L. F. de Carvalho, E. Carrilho, O. M. Bruno, M. E. Melendez, and O. N. Oliveira, "Detection of a sars-cov-2 sequence with genosensors using data analysis based on information visualization and machine learning techniques," *Mater. Chem. Front.*, vol. 5, pp. 5658–5670, 2021.

[33] M. Tang, M. Zhang, L. Xia, Z. Yang, S. Yan, H. Wang, D. Wei, C. Du, and H.-L. Cui, "Detection of single-base mutation of dna oligonucleotides with different lengths by terahertz attenuated total reflection microfluidic cell," *Biomed. Opt. Express*, vol. 11, pp. 5362–5372, Sep 2020.

[34] C.-T. Lin, P. T. K. Loan, T.-Y. Chen, K.-K. Liu, C.-H. Chen, K.-H. Wei, and L.-J. Li, "Label-free electrical detection of dna hybridization on graphene using hall effect measurements: revisiting the sensing mechanism," *Advanced Functional Materials*, vol. 23, no. 18, pp. 2301–2307, 2013.

[35] E. L. S. Wong and J. J. Gooding, "Charge transfer through dna: A selective electrochemical dna biosensor," *Analytical Chemistry*, vol. 78, no. 7, pp. 2138–2144, 2006.

[36] S. Chen, Y. Sun, Y. Xia, K. Lv, B. Man, and C. Yang, "Donor effect dominated molybdenum disulfide/graphene nanostructure-based field-effect transistor for ultrasensitive dna detection," *Biosens Bioelectron*, vol. 156, p. 112128, 2020. Chen, Shuo Sun, Yang Xia, Yaping Lv, Ke Man, Baoyuan Yang, Cheng eng England 2020/03/17 06:00 Biosens Bioelectron. 2020 May 15;156:112128. doi: 10.1016/j.bios.2020.112128. Epub 2020 Mar 3.

[37] A. Zanobini, B. Sereni, M. Catelani, and L. Ciani, "Repeatability and reproducibility techniques for the analysis of measurement systems," *Measurement*, vol. 86, pp. 125–132, 2016.

[38] H. A. Osman and S. Shirmohammadi, "Machine learning in measurement part 2: Uncertainty quantification," *IEEE Instrumentation & Measurement Magazine*, vol. 24, pp. 23–27, May 2021.

[39] S. Shirmohammadi and H. A. Osman, "Machine learning in measurement part 1: Error contribution and terminology confusion," *IEEE Instrumentation & Measurement Magazine*, vol. 24, pp. 84–92, Apr. 2021.

[40] A. Niculescu-Mizil and R. Caruana, "Predicting good probabilities with supervised learning," in *Proceedings of the 22nd International Conference on Machine Learning*, ICML '05, (New York, NY, USA), p. 625–632, Association for Computing Machinery, 2005.

[41] L. Mi, H. Wang, Y. Tian, H. He, and N. Shavit, "Training-free uncertainty estimation for dense regression: Sensitivity as a surrogate," 2019.

[42] J. Gawlikowski, C. R. N. Tassi, M. Ali, J. Lee, M. Humt, J. Feng, A. Kruspe, R. Triebel, P. Jung, R. Roscher, *et al.*, "A survey of uncertainty in deep neural networks," *arXiv preprint arXiv:2107.03342*, 2021.

[43] B. Lakshminarayanan, A. Pritzel, and C. Blundell, "Simple and scalable predictive uncertainty estimation using deep ensembles," in *Proceedings of the 31st International Conference on Neural Information Processing Systems*, NIPS'17, (Red Hook, NY, USA), p. 6405–6416, Curran Associates Inc., 2017.

[44] O. J. Burton, V. Babenko, V.-P. Veigang-Radulescu, B. Brennan, A. J. Pollard, and S. Hofmann, "The role and control of residual bulk oxygen in the catalytic growth of 2d materials," *The Journal of Physical Chemistry C*, vol. 123, pp. 16257–16267, June 2019.

[45] FormFactor, *Infinity Probe® Mechanical Layout Rules*, 2 2022.

[46] T. Cusati, G. Fiori, A. Gahoi, V. Passi, M. C. Lemme, A. Fortunelli, and G. Iannaccone, "Electrical properties of graphene-metal contacts," *Scientific Reports*, vol. 7, July 2017.

[47] L. Anzi, A. Mansouri, P. Pedrinazzi, E. Guerriero, M. Fiocco, A. Pesquera, A. Centeno, A. Zurutuza, A. Behnam, E. A. Carrion, E. Pop, and R. Sordan, "Ultra-low contact resistance in graphene devices at the dirac point," *2D Materials*, vol. 5, p. 025014, Feb. 2018.